High Accuracy Synchronization for Distributed Massive MIMO using White Rabbit

Thomas Bigler, Albert Treytl
Department for Integrated Sensor Systems
Danube University Krems
Viktor Kaplan Straße 2, 2700 Wr. Neustadt, Austria
{thomas.bigler, albert.treytl}@donau-uni.ac.at

David Löschenbrand, Thomas Zemen
AIT - Austrian Institute of Technology
Security & Communication Technologies
Giefinggasse 4, 1210 Vienna, Austria
{david.loeschenbrand, thomas.zemen}@ait.ac.at

***Abstract*—Accurate synchronization is a crucial prerequisite for wireless communication systems and in particular for spatially distributed massive multiple-input multiple-output (MIMO) systems or the upcoming 5G mobile communication standard. Many applications based on MIMO transmission, such as communication systems or beamforming methods, require synchronization accuracy in the low sub-nanosecond range which surpassed the capabilities of current off-the-shelf system. Furthermore, many of the currently used methods are susceptible to external influences such as temperature or mechanical stress. This paper defines the requirements for such systems and discusses the suitability of some existing synchronization and syntonization solutions. A direct frequency distribution approach using coaxial cables and the White Rabbit timing system using optical fiber is then compared in practical setups. Measurements were conducted under temperature stress to evaluate the performance of the synchronization parameters and their influence on the massive MIMO system.**

I. Introduction

Accurate synchronization is a crucial building block for the development and deployment of wireless communication systems. Massive MIMO is widely considered to be key enabler for the new 5G mobile communication standard [1]. The technology relies heavily on accurate synchronization that surpasses the capabilities of current off-the-shelf systems. The usage of a large number of radio frequency (RF) front-ends (in the order of hundreds to thousands) in a MIMO system reduces small-scale fading significantly while increasing spectral and power efficiency. To fully exploit the promising capabilities of a massive MIMO system, it should be operated in rich scattering environments where the large number of reflected and superimposed paths ensures low channel correlation. This means that the channels from one user equipment (UE) to the multitude of base station (BS) antennas differ significantly from each other. Distributing the RF front-ends in space (widely known as *distributed massive MIMO*) is a straightforward way to guarantee low channel correlation since every RF front-end fundamentally sees different scatterers. However, this spatial distribution entails the difficulty of synchronizing all components.

To the best of the authors knowledge, current state-of-the-art massive MIMO testbeds, e.g. [2], [3], use coaxial cables to distribute synchronization signals from a master clock source to slave devices and, subsequently, to the RF front-ends. Although the coaxial cables lengths (and therefore the placement of the RF front-ends) are typically variable, there are physical limits on the maximum extent. Damping, environmental distortions and propagation impairments are proportional to the length of the cables and pose a limit on synchronization signal quality. Alternatively, another approach [4] does not rely on cabled synchronization at all. The authors rather propose an over-the-air synchronization protocol that scales well with the network size. However, this method introduces additional signaling overhead and uses a wired backhaul data connection without exploring the possibility to also utilize the backhaul network for synchronization. Since an optical fiber based system could solve many of these limitations and in addition bring some advantages, the characteristics of the White Rabbit (WR) timing system, developed at CERN for high-accurate synchronization of sensor and actuator nodes, seem to be very appealing also for this application area.

In section II various use-cases for massive MIMO systems and their requirements on synchronization are investigated. Section III compares methods for synchronization and introduces the WR framework. We then evaluate the proposed method in comparison to a coaxial cable based setup in two extensive measurement campaigns in section IV. Finally, section V shows clear advantages of the proposed method and investigates further improvements to widen the scope of applications.

II. Requirements and Challenges

Considering a simple single-input single-output (SISO) link in an LTE-like OFDM system with a flat fading channel and without inter-symbol interference, then the signal model for a single subcarrier then reads as

$$y(t) = h(t)x(t) + z(t) \tag{1}$$

with the received symbol $y(t)$ equal to the transmit symbol $x(t)$ times the channel $h(t)$ plus circularly symmetric complex gaussian noise $z(t)$. The time dependency of the signal model is denoted by t.

Based on this signal model, we consider three different applications of distributed massive MIMO with varying demand on the synchronization. Figure 1 visualizes the concept of a massive MIMO system. The BS uses the large number of

RF front-ends and appropriate precoding to send the transmit signal in beams into the wireless channel such that the individual signal adds up coherently at the intended UE. The RF front-ends can be set up close to each other (collocated) or distributed with increased requirements on the synchronization system.

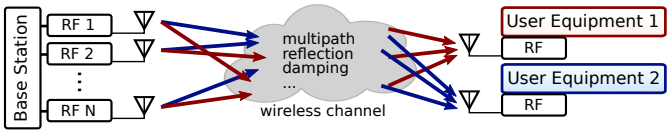

Figure 1. Basic idea of a massive MIMO system with multiple transmitters connected to one base station and multiple receivers

a) Communication System: When used as a communication system, a distributed massive MIMO system usually operates in time-division duplex (TDD) mode. Given a suitable reciprocity calibration, this allows to use uplink pilots (from UE to BS) in the downlink (from BS to UE). The TDD scheduling requires a pulse per second (PPS) synchronization performance such that uplink and downlink mode start synchronously on all RF front-ends. For a software-defined radio (SDR) testbed currently in use (e.g. [3]), the chip clock rate is around 200 MS/s. The required PPS resolution is therefore 5 ns. Moreover, timing inaccuracies up to the cyclic prefix length of the orthogonal frequency-division multiplexing (OFDM) system are compensated by channel estimation in the receivers.

If there is a carrier frequency offset between receivers at the BS, the orthogonality between subcarriers is lost and inter-carrier interference is introduced. For Long-Term Evolution (LTE)-like systems, a frequency error below $\pm$ 0.1 ppm is tolerable [5]. This translates to a required synchronization accuracy of $\pm$ 100 ns.

b) Channel Sounding: Measurement of the time-variant properties of wireless channels (*channel sounding*) is fundamental for the development and deployment of wireless communication systems [6]. The goal is to characterize the properties of the channel with as little influence of the measurement equipment as possible. In a multitone frequency channel sounder, the channel is exited with a known transmit sequence at specific frequencies. The receiver (or several receivers in a massive MIMO system) compares the received signal with the known transmit sequence and estimates the channel impulse response. If we only consider one tone of the multitone signal, (1) discribes the input output relationship of the system. Since the transmit symbol $x(t)$ is known at the receiver, it can calculate the frequency flat channel $h(t)$ by multiplication with the conjugate complex $y^*(t)$ and suitable normalization. Suppose the transmitter clock reference deviates from the (static) receiver clock reference and causes a carrier frequency offset Δf_c, the resulting transmit signal $x(t)e^{-i2\pi\Delta f_c t}$ exhibits a time dependent phase drift that is unknown to the receiver. It thus appears to originate from the channel $h(t)$ or from a moving transmitter and distorts the measurement. To reach a carrier frequency offset $\Delta f_c < 0.167$ Hz (which allows to measure velocities of the transmitter with an accuracy of 0.01 m/s at 5 GHz), the synchronization accuracy must be lower than 33 ps.

c) Beamforming and Angle-of-Arrival: The large number of RF front-ends in massive MIMO systems enables high resolution beamforming in both up- and downlink. With exact knowledge of the antenna placement, the angle of arrival of received signals can be estimated. The resolution of the estimation depends on the number of antennas, their placement and the phase accuracy of the receivers. Considering a carrier frequency f_c and corresponding wavelength λ_c and a spacing of $\lambda_c/2$ between consecutive antennas, the phase difference of a signal transmitted from a distance $\gg \lambda_c$ and angle θ is $\Delta\phi = \frac{\lambda_c \pi \cos(\theta)}{2}$. A simple reformulation gives an estimator of the angle of arrival based on the received phase difference, i.e. $\theta = \cos^{-1}\left(\frac{2\Delta\phi}{\pi\lambda_c}\right)$. It is easily verified that small phase differences $\Delta\phi$ created by synchronization clock drifts result in large angle of arrival estimation errors. To achieve 15 ° accuracy of the angle estimation at a carrier frequency of 5 GHz, the phase difference $\Delta\phi$ due to clock drifts must be smaller than 1.4 ° (0.0244 rad). Thus, a synchronization accuracy of 0.8 ps is required.

III. Frequency and Time Distribution Methods

Several methods exist for synchronization of spatially separated nodes, as used in massive MIMO systems. This section first gives a brief overview of some currently available methods and summarizes the strengths and limitations compared to the WR timing system, facilitated in this work.

a) Direct Frequency Transfer Using Coaxial Cables: A common method to achieve frequency transfer between nodes is based on coaxial cables and clock buffers which achieves good jitter performance. As the (clock) data is only transferred from transmitters to the receivers, no direct feedback on the phase difference between clock source and nodes is available. Instead, the signal phase is defined by the propagation time, and therefore by the variable length of the coaxial cable.

The basic formula for calculation of the signal phase can be written as $\Phi = 2\pi f \cdot t_p$ with $t_p = l\sqrt{\epsilon_r}/c_0$, where t_p is the propagation time, l the cable length, c_0 the velocity of light in vacuum, f the signal frequency and ϵ_r the dielectric constant of the specific coax cable material. Consequently, in order to match the phase at multiple nodes, it is mandatory to have matched cable lengths as well as equal propagation properties. The first requirement can be addressed relatively easily by using commercially available trimmed cables. However, the requirement for the equal propagation properties heavily depends on external parameters such as temperature or mechanical stress [7], which becomes increasingly important with longer cables. Existing publications show that a phase offset between source and receiver of several pico-seconds per meter has to be expected, depending on the specific coaxial cable material [8].

b) Packet-Based Synchronization: In contrast to direct frequency transfer, another possibility to synchronize multiple

nodes is a packet based approach. This requires a point-to-point communication topology where two nodes (termed master and slave) exchange packets over the communication link in order to synchronize time and frequency (syntonization). This packet exchange combined with accurate timestamps at the transmitter units allows to measure the propagation time during operation and can therefore dynamically adjust for externally induced effects on the cable. The IEEE 1588 Precision Time Protocol (PTP) is often used here [9]. The accuracy and resolution of the drawn time-stamps is one of the key properties towards highly accurate synchronization in packet bases systems. Furthermore, a signal phase-estimation and tracking is required in order to achieve timestamps below the single-shot resolution [10]. In the case of coaxial cables, it was emphasized that clock (data) transfer only takes place in one direction. Depending on the transmission media and physical layer implementation, this is different for packet based approaches where separate transmit and receive channels might exist. This causes a potential asymmetry that cannot be measured and compensated by the synchronization protocol. As an example, the ANSI/TIA/EIA 568-B standard commonly used in computer networks (e.g., CAT5 Ethernet cables) permits an asymmetry of up to 50 ns.

c) Frequency Transfer Using Synchronous Ethernet: Another synchronization/syntonization method that brings direct frequency transfer into packet-based networks is Synchronous Ethernet (SyncE), defined in the ITU-T standard G.8262 [11]. With SyncE the transmitter clock is regenerated on the receiver side using phase-locked loop (PLL), allowing (cascaded) receivers to run with the same frequency as source. The accuracy is mainly defined by the oscillators and PLL components, similar to the approach with coax cables. But again no direct method to counteract phase wander due to changes of the transmission line is available.

d) White Rabbit Timing System: The WR system combines packet-based synchronization based on the PTP protocol with syntonization based on Synchronous Ethernet [12], [13]. It was developed to provide sub-nanosecond accuracy and pico-second precision over long optical fibers with a large number of nodes involved. Figure 2 depicts the general loopback architecture used for WR, including the delay sources involved. A PLL is used to lock the internal slave circuit to the communication clock which creates the syntonization (②). The clock adjust function block is subsequently responsible for master to slave synchronization (③), which can be divided into a part for coarse synchronization via extended PTP and a part that uses a signal phase measurement performed on the master (phase_s and phase_{mm}, ④). Using a digital implementation of Dual-Mixer Time Difference (DMTD) method allows the phase detector to achieve internal measurement accuracies in the femto-second range [14].

Nevertheless, similar to the other synchronization methods discussed in this section, also the WR timing system shows dependency on external effects, and especially temperature. One effect stems from the fact that the propagation time through the fiber depends on the wavelength, defined by

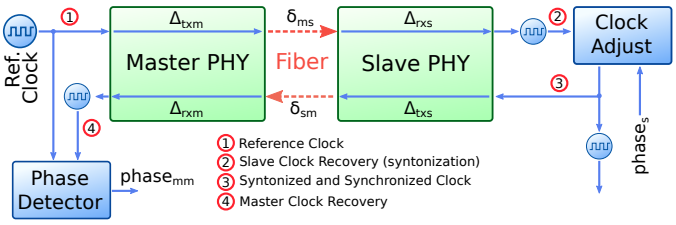

Figure 2. White Rabbit clock loopback architecture with variable and static delays of the link model

$\tau = L/c_0 \cdot (n - \lambda \cdot dn/d\lambda)$, with c_0 the speed of light in vacuum, L the fiber length, λ the wavelength and n the refractive index [15]. Both, the wavelength of the LEDs in the transmitter units as well as the refractive index of the fibers are temperature dependent, leading to a residual asymmetry that cannot be measured and compensated without external observation, e.g., by monitoring a PPS output.

According to [16] the error caused by LED wavelength are approximately 0.07 ps/(°C · km) for the 1310 nm diodes and -0.57 ps/(°C · km) for the 1490 nm diodes. Consequently, even with larger temperature changes considered, this effect only becomes relevant for longer distances. Another source for delay skews are changes on the fixed delays (Δ_{txm}, Δ_{rxs}, Δ_{rxm}, Δ_{txs}). These delays are caused by printed circuit board (PCB) traces, delays inside the FPGA or also by the electrical to optical interface. Measurements in [16] showed a temperature dependency in the range of ±10 ps/°C.

IV. Measurements

Two separate cooperative measurements were conducted. The first series focused on characterization of temperature dependency for system components, namely the coaxial cable based frequency distribution and the WR timing system. These measurements utilized a climate chamber and were carried out on the premises of the DUK. The second series of measurements, conducted at the AIT location, integrated the massive MIMO system with the goal to investigate and compare the overall application performance, again with influence of temperature changes but without climate chamber, due to logistic constraints. The measurements shown in this paper discuss temperature stress on the cable, although other cases have also been investigated. In contrast to external stress on the transceiver hardware, it is not easy to mitigate the influence on the wired transmission channel. Consequently, the cable is seen as the dominating source of environment-related phase changes in a massive MIMO system.

A. Synchronization Component Characterization

To characterize the system components, different measurement setups were used. Figure 3 shows one setup used for measurements of temperature stress on the cabling, allowing evaluation of the most critical aspects for the massive MIMO application. The temperature stress was applied using a CTS C40/200 climate chamber. The temperature inside the chamber was measured and recorded by a HTS221 temperature sensor

with a defined accuracy of ±0.5 °C, mounted on a PCB that was placed as close as possible to the devices under test. The WR switch provided the reference timing for both, the coaxial cable based direct frequency distribution and the WR communication clock. This way, the resulting jitter performance only depends on the subsequent components. The PPS signal from the switch is, on the one hand, fed into the clock splitter component OctoClock CDA-2990 and further distributed into two coaxial cables.

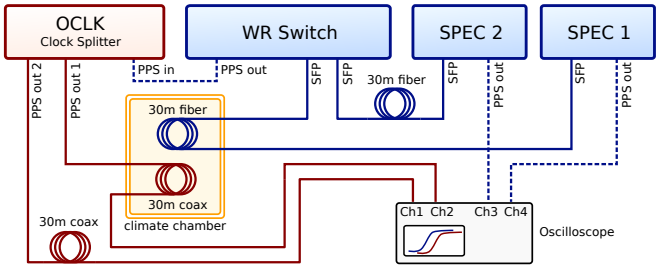

Figure 3. Setup for component characterization using a constellation with two transmit paths under temperature stress in climate chamber

On the other hand, small form-factor pluggable transceivers (SFPs) translate the electrical signal into an optical signal (and vice versa) for the fiber-optical cabling used with the WR system. Single-mode, single-strain fibers with UPC cut are connected to two Simple PCIe FMC carrier (SPEC) boards, the end-points of the WR system. In order to control and measure the temperature influence on these cards separately, both SPEC cards are operated in stand-alone mode (i.e. without installation in PCIe slots of a host). Each SPEC board is equipped with a FMC-DIO module that provides the interface logic between the FPGA on the board and LVTTL inputs and outputs. For this particular setup, the FMC-DIO default PPS output of the SPEC card is used. Each timing distribution variant (coax, fiber) uses a pair of transmission cables, where one is kept at controlled room temperature and the other one is put inside the climate chamber. In order to reduce environment effects caused by the air conditioning system or by draught, the cables that should be kept at room temperature are thermally shielded by storing them into a closed box. Similar measures to reduce undesired influences were also taken for the SPEC boards, in which case it was of course necessary to wait for a steady state due to their self-heating. Finally, for evaluation of PPS offset and jitter a LeCroy (Teledyne) WavePro 7300A oscilloscope was used. This oscilloscope provides a bandwidth of 3 GHz and a sampling rate of 20 GS/s with two active channels. When using all four channels, the maximum sampling rate is reduced to 10 GS/s. Consequently, the single-shot resolution is 50 ps and 100 ps, respectively. With the expected jitter in ps range, it is important to determine the uncertainty introduced by the oscilloscope itself. For the WavePro 7300A a standard deviation of approximately 25 ps was measured.

Figure 4 depicts a comparison measurement between direct frequency distribution and the WR system using this setup. The dashed brown curve shows the measured temperature inside the climate chamber. The red line indicates the offset between the PPS signal from the coaxial cable (channel 1 and 2 at the oscilloscope) and the blue line the PPS offset for the WR system. Both curves where filtered with a moving average filter. It can be clearly seen how the coaxial cable based system is affected by the temperature change while the WR system is able to keep the offset at an almost constant level.

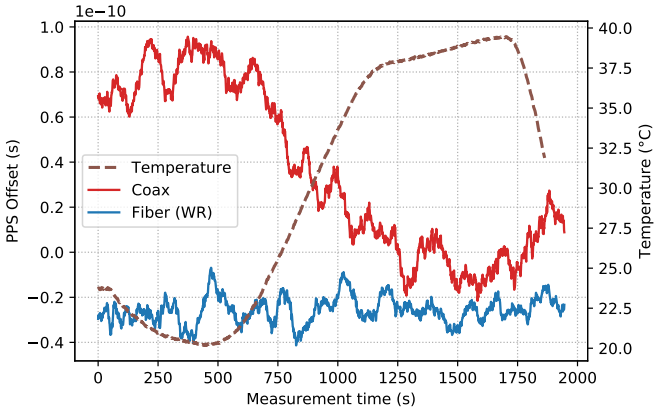

Figure 4. PPS offset wander of coaxial and optical fiber cables under temperature stress

B. System Level Characterization

In contrast to the system characterization (see IV-A), this series of measurements examined the suitability of the WR timing system for massive MIMO applications and compared it with the current technology using coaxial cables. Therefore, additional equipment was added to the measurement setup, namely a USRP-2954R SDR platform. For measurement of output signals a Keysight DSO6004A oscilloscope with a maximum sample rate of 20 GS/s and a bandwidth of 6 GHz was used. Additionally, the WR gateware (FPGA configuration) was modified to provide a 10 Mhz output signal, phased locked to the PPS output.

Again, it was important to accurately determine the uncertainties that are introduced by the measurement equipment and the signal sources. Table I contains a jitter analysis with the WR switch providing the 10 Mhz reference clock for all components. The first two lines show the jitter when measuring the 10 MHz signal directly from the WR switch and the (synchronized) WR SPEC board. If these values are compared with those measured with the WavePro 7300A oscilloscope, the lower signal variance is clearly evident. Furthermore, it also shows that the clock signal of the WR switch is much more stable than for the WR SPEC board, an issue that presumably is caused by the controlled oscillator on the WR SPEC board. This was also visible at the component characterization measurements, but due to the limits of the LeCroy oscilloscope not as distinct as here.

Row three and four show the jitter when a CDA-2990 clock buffer (termed OCLK) is placed between WR component and oscilloscope, which clearly reduces the measured jitter. As a

Table I
JITTER ANALYSIS OF WR COMPONENTS

#	Measurement at DSO6004A	σ
1	WR Switch	5.7 ps
2	WR SPEC	20.0 ps
3	WR Switch → OCLK1	1.87 ps
4	WR SPEC → OCLK3	2.69 ps
5	WR Switch → OCLK1 → 30 m Coax → OCLK2	3.0 ps
6	Rubidium Standard	15.5 ps

clock buffer only maps the (digital) input signal to a defined output level, this improvement can be explained by the cleaner and steeper signal edges seen by the oscilloscope. Row five addresses a setup with two clock buffers and a 30 m coaxial cable in series where the jitter is slightly increased. Finally, the last row depicts the jitter analysis of a GPS10eR Ultra Low Noise Rubidium frequency standard. The clock jitter is approximately three times higher than at the WR switch directly and also underlines why the WR switch was not externally disciplined by the Rubidium for these particular measurements.

Figure 5 illustrates one measurement setup that was used to investigate the impact of the WR clock jitter on the massive MIMO application. The WR SPEC boards are synchronized to the WR master using 30 m optical fiber cables and provide (phase locked) 10 MHz and 1 PPS signals to the clock buffers OCLK1 and OCLK3. Clock buffer OCLK1 further distributes both signals directly to USRP TX and USRP RX1 (shown as one function block) and, over 30 m coaxial cables, to OCLK2 which sources USRP RX2. SPEC2 provides the timing signals to OCLK3 and subsequently to USRP3. The USRP SDR TX transmit a single tone at 5.2 GHz which is received by the USRPs (RX1 to RX3). The phase of the received tones is then recorded and stored for offline-analysis. As USPR RX1 is connected to the WR SPEC boards with short cables and not influenced by external stress it can be interpreted as reference receiver.

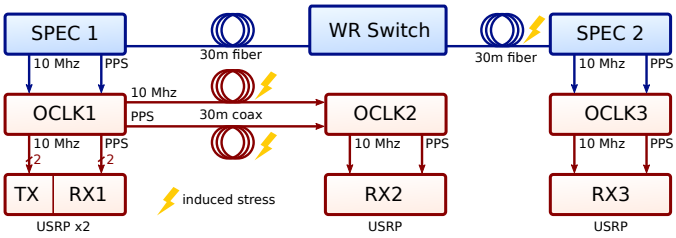

Figure 5. Measurement setup

Controlled temperature stress is applied onto the cables using a closed box, which is either heated up by a hot-air gun or cooled down using ice. The affected connections were marked with a flash symbol in Figure 5. The temperature is again measured using the HTS221 sensor board placed close to the cables. Figure 6 depicts such a measurement with the cables first cooled down and then heated up to approximately 40 °C. While the heating control works quite well with a human on/off controller, cooling happens rather uncontrolled. Nevertheless, for these measurements the exact temperature is secondary as the cable core temperature cannot be determined with non-destructive methods anyway. The result of this measurement is illustrated in Figure 6 with the brown dashed lines representing the measured temperature and the red and blue lines for measured phase at the USRPs RX2 and RX3, representing the coaxial cable based and WR timing system. For better comparison, the initial offset of the phase measurements was removed, having both curves start at zero phase.

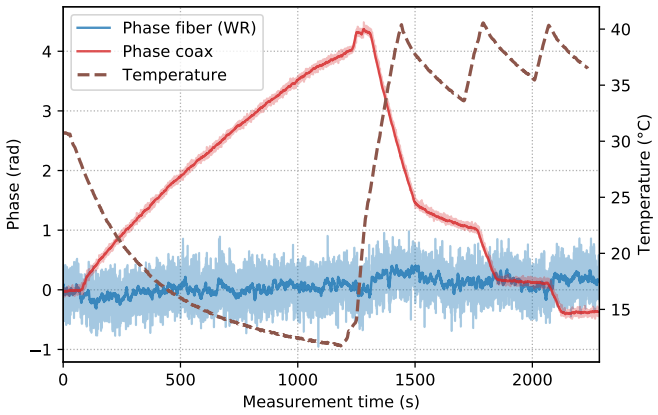

Figure 6. Normalized phase wander of transmitted signal in relationship to temperature influence on fiber (White Rabbit) and coax cables

For both, the raw phase values (light colors) and a filtered version (dark colors) are plotted. As with the component characterization measurements, the temperature dependency of the coaxial cable is clearly visible. When cooling down the phase of the coax cable signal changes more the 4 rad, resulting in a phase wrap which is not shown in this figure. On the other hand, the phase of the WR system is almost unaffected by temperature, but shows distinct phase noise with a peak-to-peak value of approximately 1 rad and standard deviation of 0.2 rad. In comparison, the coax system only shows a measured standard deviation of roughly 0.03 rad.

To visualize how the WR timing system compensates the temperature influence on the optical fiber, Figure 7 shows the measured master-to-slave delay and the phase setpoint value phase_s applied at the slave for compensation (see also Figure 2).

The findings from the phase measurements differ from the jitter analysis in Table I where similar phase noise was measured when using the clock buffers. Therefore, the type and source of the measured noise was investigated in more detail using filters and frequency-domain analysis methods. These investigations showed that most of the signal power is located below 50 Hz with an additional peak at approximately 270 Hz. Filtering signal components below 100 Hz improves phase noise performance as illustrated in Figure 8. The upper part of Figure 8 shows the unfiltered data of the WR system

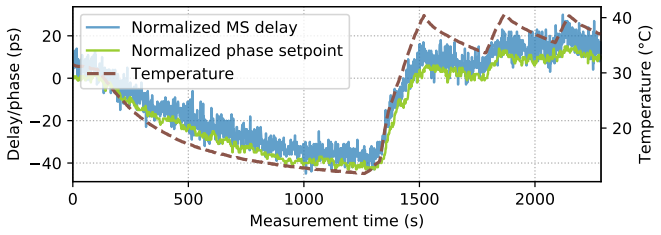

Figure 7. Normalized measurement of master-to-slave delay and phase setpoint from White Rabbit timing system

phase and the lower part the version with applied high-pass filter. We assume that these frequency components originate from the controller implementation in the slave, but further investigations are necessary to verify this and to develop solutions to improve the properties of the WR system for massive MIMO systems.

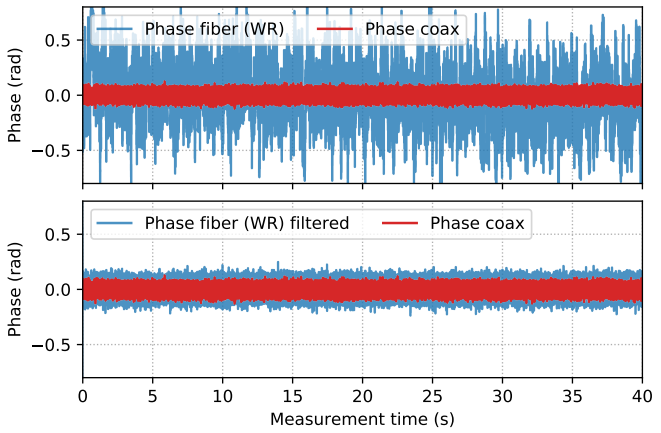

Figure 8. Comparison of raw and high pass filtered (cutoff 100Hz) WR phase to coaxial phase at constant temperature

This also reveals the reason why the results of the WR jitter measurements are similar to those of direct frequency distribution, while the phase measurements are visibly worse. Jitter is measured for very short time periods while the effect seen here is rather slow.

V. Conclusion and Outlook

The measurements conducted show that the WR system with the current implementation of the WR SPEC boards is not suitable for all the applications of (massive) MIMO, which are outlined in chapter II. Although the jitter performance is acceptable for communication and channel sounding systems, the requirements of beamforming and angle-of-arrival systems cannot be fully met. Nevertheless, it was also shown that WR provides several advantages over synchronization systems based on direct frequency distribution. One advantage is the high immunity against cable temperature changes which leads to large phase wander in coaxial cable based systems. Additionally, with WR it is also possible to use the optical fiber link for regular high bandwidth data exchange, a feature that is particularly valuable for spatially distributed nodes.

It has also been shown that the high phase noise of the WR system is generated by rather low-frequency components. The source of this frequency components needs to be further investigated but presumably stems from the oscillator frequency control algorithm at the slave. Consequently, several options are feasible to improve the clock noise, such as modification of the control algorithm (e.g. lowering the loop bandwidth) or clock cleaner components. It also should be mentioned that a new revision of the WR SPEC board is currently planed, which might further improve the default synchronization accuracy and precision.

References

[1] E. G. Larsson, O. Edfors, F. Tufvesson, and T. L. Marzetta, "Massive mimo for next generation wireless systems," *IEEE Communications Magazine*, vol. 52, no. 2, pp. 186–195, February 2014.

[2] C. Shepard, H. Yu, N. Anand, E. Li, T. L. Marzetta, R. Yang, and L. Zhong, "Argos: practical many-antenna base stations," no. i, 2012, p. 53.

[3] S. Malkowsky, J. Vieira, L. Liu, P. Harris, K. Nieman, N. Kundargi, I. C. Wong, F. Tufvesson, V. Owall, and O. Edfors, "The World's First Real-Time Testbed for Massive MIMO: Design, Implementation, and Validation," *IEEE Access*, vol. 5, no. DL, pp. 9073–9088, 2017.

[4] R. Rogalin, O. Y. Bursalioglu, H. Papadopoulos, G. Caire, A. F. Molisch, A. Michaloliakos, V. Balan, and K. Psounis, "Scalable synchronization and reciprocity calibration for distributed multiuser MIMO," *IEEE Transactions on Wireless Communications*, vol. 13, no. 4, pp. 1815–1831, 2014.

[5] 3GPP, "Evolved Universal Terrestrial Radio Access (E-UTRA); Base Station (BS) radio transmission and reception," 3rd Generation Partnership Project (3GPP), Technical Specification (TS) 36.104, 07 2010, version 9.4.0. [Online]. Available: http://www.etsi.org/deliver/etsi_ts/136500_136599/13652101/14.02.00_60/ts_13652101v140200p.pdf

[6] A. F. Molisch, *Wireless Communications*, 2011.

[7] Z. Konečná, "Temperature dependence of electrical parameters of coaxial cables," in *2016 Conference on Diagnostics in Electrical Engineering (Diagnostika)*, Sept 2016, pp. 1–4.

[8] K. Czuba and D. Sikora, "Temperature Stability of Coaxial Cables," in *Physical Aspects of Microwave and Radar Applications*, vol. 119, no. 4, 2011, pp. 553 – 557.

[9] J. C. Eidson, *Measurement, Control, and Communication Using IEEE 1588*. Springer, 2006.

[10] P. Loschmidt, R. Exel, and G. Gaderer, "Highly Accurate Timestamping for Ethernet-Based Clock Synchronization," *Journal of Computer Networks and Communications*, vol. 2012, p. 11, 2012.

[11] K. Hann, S. Jobert, and S. Rodrigues, "Synchronous ethernet to transport frequency and phase/time," *IEEE Communications Magazine*, vol. 50, no. 8, pp. 152–160, August 2012.

[12] M. Rizzi, M. Lipiński, T. Wlostowski, J. Serrano, G. Daniluk, P. Ferrari, and S. Rinaldi, "White rabbit clock characteristics," in *2016 IEEE International Symposium on Precision Clock Synchronization for Measurement, Control, and Communication (ISPCS)*, Sept 2016, pp. 1–6.

[13] M. Lipiński, T. Włostowski, J. Serrano, and P. Alvarez, "White rabbit: a ptp application for robust sub-nanosecond synchronization," in *2011 IEEE International Symposium on Precision Clock Synchronization for Measurement, Control and Communication*, Sept 2011, pp. 25–30.

[14] P. Moreira, P. Alvarez, J. Serrano, I. Darwezeh, and T. Wlostowski, "Digital dual mixer time difference for sub-nanosecond time synchronization in ethernet," in *2010 IEEE International Frequency Control Symposium*, June 2010, pp. 449–453.

[15] P. O. Hedekvist and S.-C. Ebenhag, "Time and frequency transfer in optical fibers," in *Recent Progress in Optical Fiber Research*, S. W. Harun, Ed. Rijeka: InTech, 2012, ch. 17. [Online]. Available: https://doi.org/10.5772/27345

[16] H. Li, G. Gong, W. Pan, Q. Du, and J. Li, "Temperature effect on white rabbit timing link," *IEEE Transactions on Nuclear Science*, vol. 62, no. 3, pp. 1021–1026, June 2015.